Optical and Quantum Electronics (2022) 54:20
https://doi.org/10.1007/s11082-021-03411-y

Spin–orbit coupling effect on electronic, linear and nonlinear optical properties of Bi_2S_3 and the ternary bismuth sulfide $Bi_2S_{2.75}Se_{0.25}$: Ab-initio calculations

H. Ben Abdallah[1] · **W. Ouerghui**[2]

Received: 19 July 2021 / Accepted: 18 November 2021 / Published online: 29 November 2021

Abstract
Although the relevant properties of the bismuthinite Bi_2S_3, it was recently approved that the substitution of Se atoms in the Bi_2S_3 lattice can significantly enhance its electro-optical properties. In the present work, a detailed study on the structural, electronic and optical properties of $Bi_2S_{2.75}Se_{0.25}$ has been carried out based on first principle calculations. The simultaneous effect of Se-doping and spin–orbit coupling (SOC) on bismuth sulfide Bi_2S_3 was investigated. Our calculations show that $Bi_2S_{2.75}Se_{0.25}$ exhibits a narrow direct band gap of 1.062 eV after inclusion of the (SOC). The calculation of the carrier effective masses indicates that $Bi_2S_{2.75}Se_{0.25}$ may possess a high electron mobility material which is in accordance with experimental studies. The linear absorption optical spectra for both Bi_2S_3 and $Bi_2S_{2.75}Se_{0.25}$ show that doping bismuthinite with (Se) increases the optical absorption coefficient in the visible range and takes a value up to 1010^5 cm^{-1}. In addition, the dielectric function, optical conductivity and the energy loss function of Bi_2S_3 and $Bi_2S_{2.75}Se_{0.25}$ were also derived. The addition of the (Se) content induces a red shift in agreement with experimental studies. A noticeable effect of the (SOC) on the linear optical parameters was observed. The stability of the excitons was also studied by the estimation of the binding energy value. The dispersion energy parameters of Bi_2S_3 and $Bi_2S_{2.75}Se_{0.25}$ were estimated using a single oscillator model. Some nonlinearities have been computed with and without inclusion of (SOC) showing that $Bi_2S_{2.75}Se_{0.25}$ with large nonlinear optical parameters is promising candidate in photonic switching applications.

Keywords Electronic structure · Optical properties · Spin–orbit coupling · Bismuth sulfide

✉ H. Ben Abdallah
bhouda02@yahoo.fr

[1] Laboratoire de Physique de La Matiere Condensée, Département de Physique, Faculté Des Sciences de Tunis, Université Tunis El Manar, 2092 Tunis, Tunisia

[2] Laboratoire Matériaux, Molécules Et Applications, Institut Préparatoire aux Etudes Scientifiques Et Techniques, University Carthage, La Marsa 2075, Tunis, Tunisia

1 Introduction

Bismuth chalcogenide materials Bi_2X_3 (X = S, Se, Te) are considered as the second generation topological insulators as they have insulating bulk band gap and conducting states on their surface (Koc et al. 2014). Their bulk band gaps are generated because of the inherent spin–orbit coupling in these systems. The cation Bi^{3+} has a large relativistic effect and a strong sp hybridization in the valence band (Ganose et al. 2016). As a result, the Bi based materials may possess low carrier effective masses and therefore high carrier mobility leading them to be very useful in photovoltaic applications as a solar cell. Particularly, VI- bismuth materials Bi_2X_3 are functional compounds (Deng and Zhao 2018) and they are very attractive materials for several applications including: photovoltaics (Konstantatos et al. 2008), thermoelectrics (Harman et al. 2002), photo-electrochemicals (Kim et al. 2019), photocatalytic activity (Wu et al. 2010), micro- and optoelctronic devices (Hu et al. 2020) and infrared detectors (Grigas et al. 2002). Among Bi_2X_3 materials, the bismuth sulfide Bi_2S_3-bismuthinite- is a metal chalcogenide with a very attractive and intriguing properties: a large optical absorption coefficient ($> 10^5$ cm^{-1} for $\lambda < 500$ nm), high electron mobility (> 500 cm V^{-1} s^{-1}) (Rahman et al. 2016) and so on. The band gap of Bi_2S_3 is around 1.3–1.7 eV (Bernechea et al. 2015) and therefore lies in the visible light spectrum allowing it to be a light-absorber material in solar cells (Song et al. 2016). These relevant properties have allowed Bi_2S_3 to be a potential candidate for diverse domains such as photovoltaics (Whittaker-Brooks et al. 2015), thermoelectrics (Liufu et al. 2007), electrochemical hydrogen storage (Zhang et al. 2006), lithium and sodium batteries (Ellis et al. 2014), electrochemical sensors (Andzane et al. 2015), X-ray computed tomography (Rabin et al. 2006), and so on. Despite its interesting and relevant properties, the use of Bi_2S_3 in the various fields mentioned above is hampered by its large electrical resistivity (Zhang et al. 2013) in the case that it will be used as an electron acceptor and also by its short life of minority carriers when it will be used in the manufacture of solar cells To improve the efficiency of Bi_2S_3 in solar cells development and to enhance its electrical transport properties, a systematic study on the intrinsic and extrinsic defects it is crucial to optimize performances of bismuth sulfide Bi_2S_3. Several researches have carried out a comprehensive study on intrinsic defects and doping in Bi_2S_3. For example, Mizoguchi et al. (1995) found that S vacancies in the lattice of bismuthinite can reduced its electrical resistivity by 2–3 orders of magnitude. Similarly, doping Bi_2S_3 by substitutional extrinsic elements such as Cl (Du et al. 2014), Sb (Kawamoto and Iwasaki 2014), Cu (Ge et al. 2012), Ag (Yu et al. 2011), Eu (Zhang et al. 2017) and Mn (Anasane and Ameta 2017) has been found to optimizing its carrier concentration so improving its electrical properties. Recently, much experimental reports have shown that the introducing selenium atoms to Bi_2S_3 can be considered as a very efficient way to increase its electrical and optoelectronic properties. It has shown that Se alloying bismuthinite in S sites ($Bi_2S_{2.85}Se_{0.15}$) could increase a figure of merit (ZT) and enhance the thermal conductivity upon Se incorporation (Zhang et al. 2013). Ajara et al. (Rahman et al. 2016) have found that ($Bi_2S_{3-x}Se_x$) solid solutions possess interesting and attractive electrical properties than Bi_2S_3. Recently, experimental investigations conducted by Ye Chen et al. (2019) show that the power factor in the case of Se alloying at S sites in Bi_2S_3 is about 100 times larger than that of undoped Bi_2S_3. $Bi_2S_{3-x}Se_x$ can be also an all-optical photonics switching device due to its interesting non-linear optical properties (Shubar et al. 2020). Photocatalytic activity can be highly increased when doping selenium into Bi_2S_3 photocatalyst (Song et al. 2011). It has also been proved that Se-doped Bi_2S_3 can be used as anodes for sodium-ion batteries (Chen et al. 2020). In contrast, to our

knowledge no theoretical study has been reported to date to investigate changes in electro-optical properties caused by the substitution of Se atoms into Bi_2S_3. For this purpose, our study is focused on predicting the structural, electronic and optical properties of $Bi_2S_{3-x}Se_x$ ($x=0$ and 0.25). The calculations were carried out using ab initio density functional theory (DFT) employing the Full-Potential Linearized Plane Wave (FP-LAPW) method. In the present paper we also discussed the effect of the spin–orbit coupling (SOC) on the electro-optical properties for Bi_2S_3 and the ternary bismuth sulfide $Bi_2S_{2.75}Se_{0.25}$.

2 Computational details

In the present study, the full potential linearized plane wave (FP-LAPW) method (Nordström et al. 2001) as implemented in the Ab-initio simulation Wien2k (Blaha et al. 2020) package based on the density functional theory (DFT) (Chu and Leung 2001), is used to carried out all of the calculations. Perdew-Burke-Ernzerhof (PBE-GGA) scheme was used to describe the exchange–correlation interaction (Perdew et al. 1996) in addition of spin–orbit coupling (SOC) (Bala et al. 2008). In this study, the valence electrons are: [$6s^2$ $6p^3$], [$3s^2 3p^4$] and [$4s^2 4p^4$] for Bi, S and Se atoms respectively. The potential and charge density inside the atomic spheres are taken as $l_{max}=10$. The plane wave cut-off was set at $R_{MT*}K_{max}=8$, where R_{MT} denotes the smallest muffin-tin radii of all atomic spheres and K_{max} is the largest k-vector of the reciprocal lattice. $G_{max}=12$ $(Ryd)^{1/2}$ is truncated to develop charge density and the plane wave potential. The energy cut-off for separation core and valence electrons is set to −10 Ry. A 500 k-point are used in the irreducible Brillouin zone. A denser k-mesh are used for calculation of the optical properties. The calculations are self-consistently converged when the total energy convergence was stable within 10^{-4} Ry.

3 Results and discussion

3.1 Structural properties

Bismuthinite Bi_2S_3 crystallizes in orthorhombic structure with the space group *pbnm* (62) (Caracas and Gonze 2005). There are four formula units per unit cell giving rise to 20 atoms in the primitive cell. The crystal structure of Bi_2S_3 consists of five non-equivalent atoms: two non-equivalent Bi sites and three non-equivalent S sites. Each Bi atom is linked to seven atoms of S. Three atoms of S are linked to Bi atom by short distances and the other four atoms of S are linked to Bi by long distances. The Bi–S short-bonds formed a strongly bonded ribbons while the Bi–S long-bonds formed a Van der Waals force introducing a weak interaction between the aligned ribbons (Li et al. 2016). To model the $Bi_2S_{3-x}Se_x$ structure, a 221 supercell was constructed generating eight Bi atoms and twelve S atoms in unit cell with formula Bi_8S_{12} in which three S atoms were replaced by three Se atoms to get $Bi_2S_{2.75}Se_{0.25}$. The crystal structures of Bi_2S_3 and $Bi_2S_{2.75}Se_{0.25}$ are shown in Fig. 1.

To find the ground state properties of Bi_2S_3 and $Bi_2S_{2.75}Se_{0.25}$, the variation in the total energies with volume is computed using the GGA-PBE method for different volumes about the equilibrium cell volume V_0, using the Murnaghan's equation of state (Ouerghui and Alkhalifah 2019) as demonstrated in Fig. 2. The calculated equilibrium lattice constants, the bulk modulus (B) and its derivative of pressure (B') for

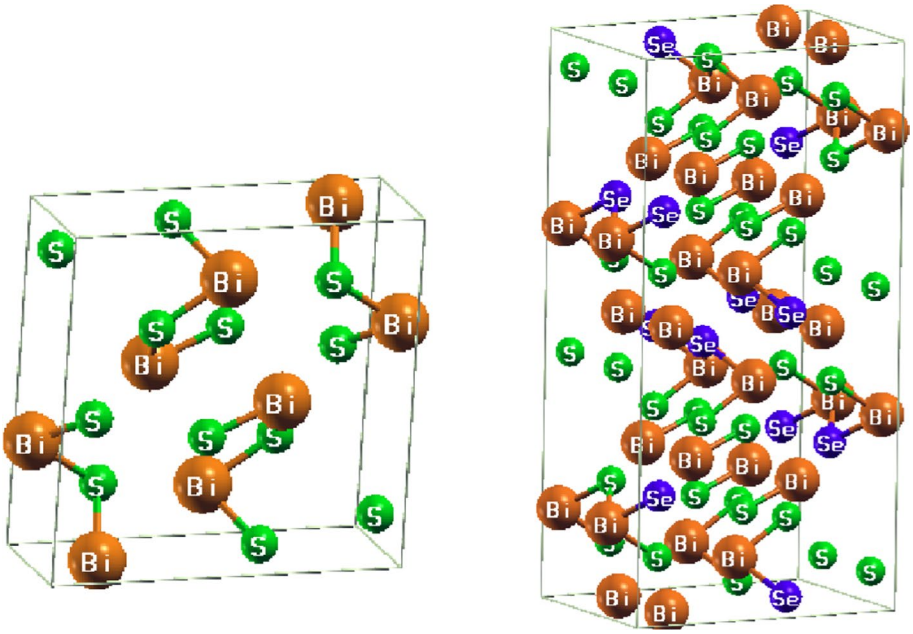

Fig. 1 The orthorhombic crystal structures of $Bi_2S_{3-x}Se_x$. (The left is the structure for x = 0 and the right for x = 0.25)

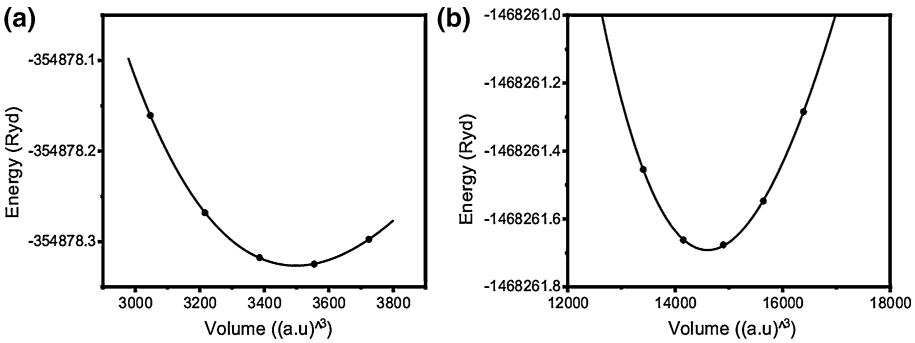

Fig. 2 Calculated total energy as a function of volume within GGA-PBE for Bi_2S_3 and $Bi_2S_{2.75}Se_{0.25}$

both compounds are given in Table 1, with other previous theoretical and experimental results. From Table 1, we see that the optimized lattice parameters for bismutinite Bi_2S_3 are in good agreement with theoretical results and slightly higher than the experimental data since the GGA approximation overestimates the lattice constants. In addition, the lattice constants increase with adding Se in the Bi_2S_3 lattice which can be explained by ionic radii difference between S^{2-} (1.81 Å) and Se^{2-} (1.98 Å).

Table 1 Optimized lattice constants, bulk modulus B and its pressure derived B' and other available experimental data and theoretical values for Bi_2S_3 and $Bi_2S_{2.75}Se_{0.25}$

Compound	Method	*a* (Å)	*b* (Å)	*c* (Å)	*B* (GPa)	*B*′
Bi_2S_3	Present (GGA-PBE)	11.428	4.024	11.268	65.297	4.450
	Theory (DFT-LDA) (Koc et al. 2014)	11.314	3.980	11.014	78.82	4.370
	Theory (DFT-GGA) (Li et al. 2016)	11.227	3.999	11.001		
	Experimental (Caracas and Gonze 2005)	11.305	3.981	11.147		
$Bi_2S_{2.75}Se_{0.25}$	Present (GGA-PBE)	11.592	4.082	11.430	63.840	2.839

3.2 Electronic properties

3.2.1 Electronic band structure

Based on the optimized lattice parameters, the electronic band structures of Bi_2S_3 and $Bi_2S_{2.75}Se_{0.25}$ were evaluated using GGA-PBE approach with and without spin–orbit coupling (SOC). Figure 3a–d show the electronic band structures plotted along the high symmetry directions for the two structures Bi_2S_3 and $Bi_2S_{2.75}Se_{0.25}$. For Bi_2S_3, Fig. 3a shows an indirect band gap with the valence band maxima (VBM) occurs at the *X*-point whereas the conduction band minima (CBM) is located along the *G-Z* direction. The calculated band gap of bismuthinite Bi_2S_3 at the PBE level is $E_g^{PBE} = 1.492$ eV which is in accordance with other theoretical and experimental results suggesting that Bi_2S_3 is an indirect band gap semiconductor ranging from 1.3–1.7 eV (Bernechea et al. 2015). It is well-known that the inclusion of the SOC effect modify the electronic properties of the materials which contain heavy elements. In our case, with the spin–orbit effect consideration, the band gap of Bi_2S_3 decreases from $E_g^{PBE} = 1.492$ eV to $E_g^{PBE+SOC} = 1.208$ eV. $E_g^{PBE+SOC}$ is also an indirect band gap with (VBM) and (CBM) are located at *Z*-point and *GY*- path respectively, which is very close to the experimental value of 1.26 eV (Chen et al. 2019). The computed energy band gaps of Bi_2S_3 at PBE and PBE + SOC levels are summarized in Table 2 within previously theoretical and experimental studies. Figure 3c, d shows the electronic band structures of $Bi_2S_{2.75}Se_{0.25}$ with and without (SOC). Both band structures present a direct band gaps of $E_g^{PBE} = 1.34$ eV and $E_g^{PBE+SOC} = 1.062$ eV at PBE and PBE + SOC level respectively at Z point. The incorporation of Se atoms in the Bi_2S_3 lattice allowed to obtain a narrow band gap leading to activate the intrinsic conduction electrons and subsequently to enhance the electrical transport properties of the undoped Bi_2S_3 material. The reduction of the band gap by introducing the Se atoms in Bi_2S_3 has been observed experimentally by studying the $Bi_2S_3 - {}_xSe_x$ (x = 0.06–0.75) materials (Biswas et al. 2012) in which the band gap passes from 1.35 to 1.12 eV. Due to the fact that the obtained gap is direct, the $Bi_2S_{2.75}Se_{0.25}$ is satisfactory in optoelectronics and also it can be considered as a light-absorber compound in solar cells due to its value that is close to the optimal value of this kind of materials (Zhu et al. 2017). The calculated band gaps $E_g^{PBE+SOC}$ for Bi_2S_3 and the ternary $Bi_2S_{2.75}Se_{0.25}$ indicate that the (SOC) induces a considerable reduction compared to the E_g^{PBE} which can be explained by the splitting states near the Fermi level.

3.2.2 Density of states

The total density of states (TDOS) and the partial density (PDOS) for Bi_2S_3 and $Bi_2S_{2.75}Se_{0.25}$ were calculated to unveil the atom orbital contribution to the band structure.

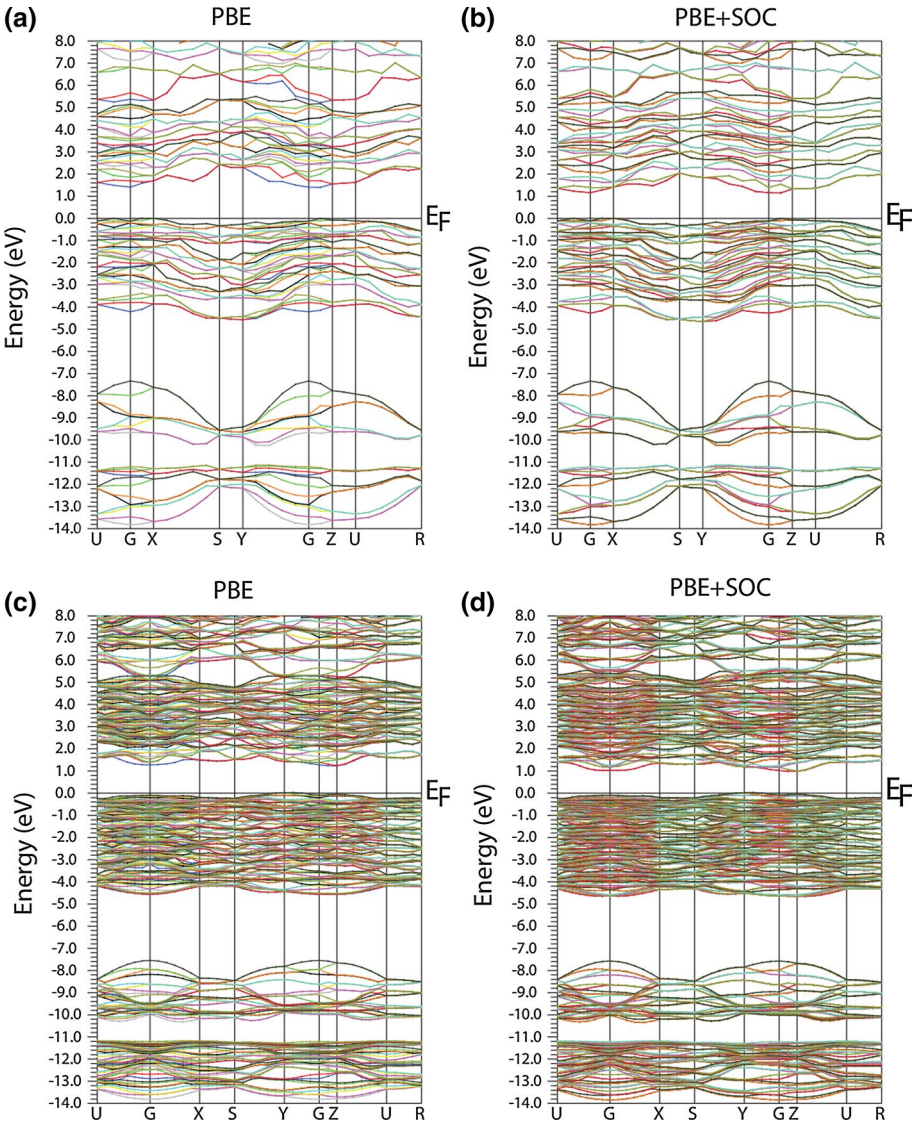

Fig. 3 Calculated electronic band structures of Bi_2S_3 (**a**, **b**) and $Bi_2S_{2.75}Se_{0.25}$ (**c**, **d**) with PBE and PBE + SOC methods

(TDOS) and (PDOS) are calculated with and without (SOC) and are presented in Figs. 4 and 5. In these figures, the zero energy level is attributed to the Fermi level (E_f). It emerges from Fig. 4 that the lower part of the valence band is dominated by the Bi-6s and S-3s states. The 3p orbitals of S atoms have highly contribution to the upper valence band showing hybridization with Bi-6sp orbitals with a weak presence of Bi-5d states. The conduction band minimum is composed principally of the Bi-6p and S-3p characters. The same orbital contributions to the energy bands of $Bi_2S_{2.75}Se_{0.25}$ are observed with the addition of the p states of Se atoms which has a considerable contribution in the valence band

Table 2 The calculated energy band gaps of Bi_2S_3 and $Bi_2S_{2.75}Se_{0.25}$ with PBE and PBE + SOC methods with their corresponding theoretical and experimental data

Compound	Method	E_g (eV)
Bi_2S_3	Present (GGA-PBE)	1.492
	Present (PBE-SOC)	1.208
	Theory (DFT-GGA and PAW) (Guo et al. 2013)	1.220
	Theory (LDA-PBE) (Chen et al. 2019)	1.380
	Theory (PBE-SOC) (Chen et al. 2019)	1.030
	Experimental (Chen et al. 2019)	1.260
	Experimental (Cheng et al. 2010)	1.360
$Bi_2S_{2.75}Se_{0.25}$	Present (GGA-PBE)	1.340
	Present (PBE-SOC)	1.062

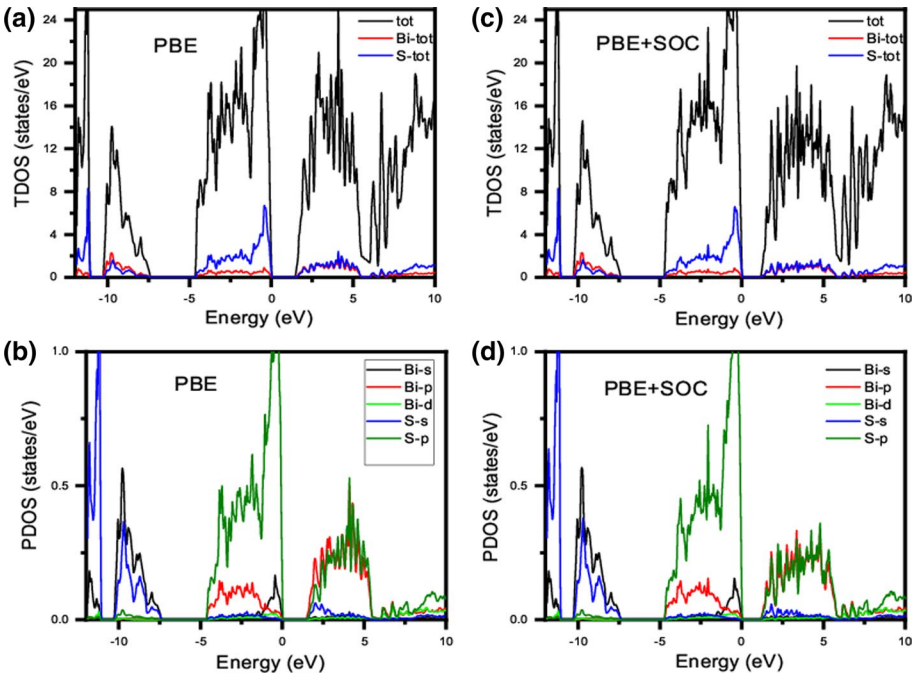

Fig. 4 Calculated total (TDOS) and partial density of states (PDOS) of Bi_2S_3 with PBE and PBE + SOC methods

maximum giving rise to the hybridization with Bi-6p orbitals. The Se 4p states contribute also in the conduction band minimum besides the p states of Bi and S atoms. After the inclusion of the (SOC), the contribution of the different states in the valence and the conduction bands remains unchanged but a remarkable reduction in their densities is observed as shown in the Figs. 4d and 5d for the two materials. We find also that the bandwidth has increased by 0.112 eV for Bi_2S_3 and by 0.086 eV for $Bi_2S_{2.75}Se_{0.25}$ in the presence of (SOC). The obtained results from the electronic band structures as well as the density of

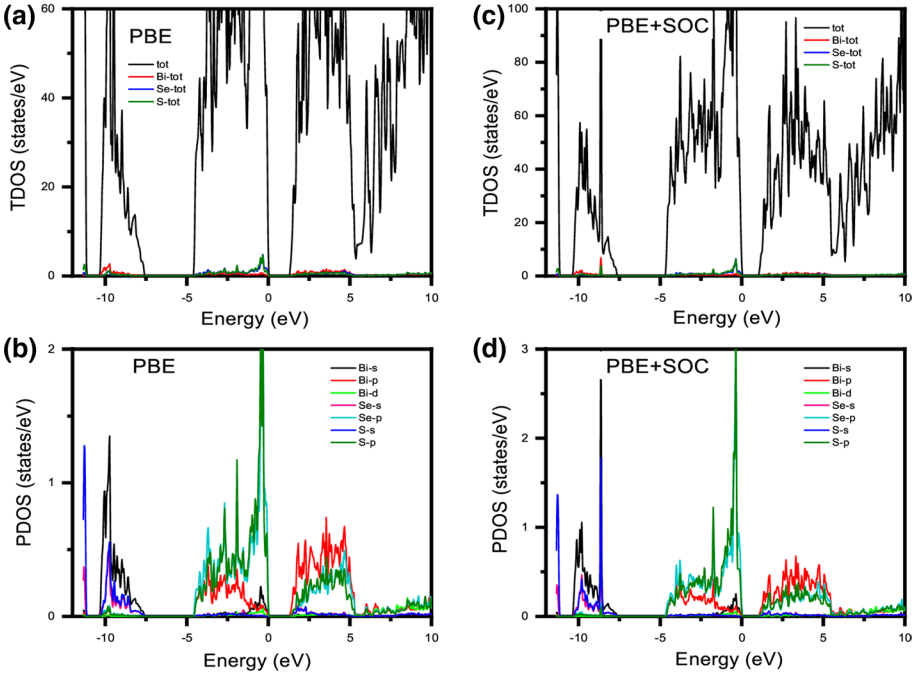

Fig. 5 Calculated total (TDOS) and partial density of states (PDOS) of $Bi_2S_{2.75}Se_{0.25}$ with PBE and PBE + SOC methods

states show the influence of the introduction of the (SOC) on the electronic structure of the undoped and doped bismutinite Bi_2S_3.

3.2.3 Effective masses

To understand the physical mechanism of the thermoelectric property of bismuthinite and the Se-doped bismuthinite (Bi_2S_3), carrier effective masses were calculated at *G*-point along *G-Z* (0, 0, 1/2) and *G-X* (1/2, 0, 0) directions in the first Brillouin zone of the *pbnm* orthorhombic structure. For the calculation of the effective masses we use the approximation model given by Ben Abdallah and Ouerghui (2020) based on the calculated band structures with PBE + SOC model. The results are depicted in Table 3. As it is presented in Table 3, the electron effective masses m_e^* for both Bi_2S_3 and $Bi_2S_{2.75}Se_{0.25}$ are smaller than the effective hole masses m_h^*, which is in accordance with the experimental and theoretical studies (Chen et al. 2019; Guo et al. 2013). For Bi_2S_3, our calculated average value of m_e^* is 1.85 m_0 consistent with the previous experimental data (Pejova and Grozdanov 2006) showing that m_e^* is ranging from 0.6 to 2.2 m_0. The carrier effective mass anisotropy can be attributed to the anisotropic ratio $\frac{m_c^*}{m_a^*}$ where m_c^* and m_a^* are the carrier effective masses along the (*G-Z*) and (*G-X*) directions respectively. The calculated electron effective mass anisotropy is 1.30 for Bi_2S_3 and 2.42 for $Bi_2S_{2.75}Se_{0.25}$. The obtained higher anisotropy is related to the chemical bonds in the two crystals. The anisotropy increased when selenium atoms were substituted in Bi_2S_3 crystal resulting in a more covalent bonds along c-axis and a weaker ionic bonds along the a and b directions. In addition, the introduction of the Se

Table 3 Calculated effective masses of electrons and holes in units of free electron mass m_0 for Bi_2S_3 and $Bi_2S_{2.75}Se_{0.25}$ along *G-X* and *G-Z* directions

System	Direction	$m_e^*[m_0]$	$m_h^*[m_0]$
Bi_2S_3	*G-Z*	2.099	3.850
	G-X	1.607	4.530
$Bi_2S_{2.75}Se_{0.25}$	*G-Z*	0.489	1.301
	G-X	1.187	2.110

atoms in bismuthinite crystal has the effect of reducing the electron and hole effective masses and thus an increase in the carrier mobility. This has been observed experimentally by Ajara et al. (Shubar et al. 2020).

3.3 Optical properties

3.3.1 Linear optical properties

The linear optical properties of Bi_2S_3 and $Bi_2S_{2.75}Se_{0.25}$ are calculated with and without (SOC) for radiation up to 12 eV as shown in Figs. 6, 7, 8, 9 and 10. All optical parameters are derived from the complex dielectric function $\varepsilon(\omega) = \varepsilon_1(\omega) + i\varepsilon_2(\omega)$ which define the optical response of a medium at all photon energy. $\varepsilon_1(\omega)$ is the real part of $\varepsilon(\omega)$ corresponds to the dispersive behavior of the material while $\varepsilon_2(\omega)$ is the imaginary part of $\varepsilon(\omega)$ describing the absorptive behavior of the medium (Ben Abdallah and Bennaceur 2009). As Bi_2S_3 and $Bi_2S_{2.75}Se_{0.25}$ crystallize in orthorhombic structure, the dielectric tensor $\varepsilon(\omega)$ have three diagonal independent components (ε_{xx}, ε_{yy}, ε_{zz}). In this paper, we have restricted our study of the optical properties for polarization parallel to the z direction ($E\|z$) which is considered as a preferential direction for enhancing electro-optical properties of Bi_2S_3 (Miller and Bernechea 2018). $\varepsilon_1(\omega)$ spectra calculated with and without (SOC) for Bi_2S_3 and $Bi_2S_{2.75}Se_{0.25}$ for ($E\|z$) are given by Fig. 6.

All $\varepsilon_1(\omega)$ curves start from the static dielectric constant $\varepsilon_1(0)$ which corresponds to the dielectric response at zero frequency. The static dielectric constants for Bi_2S_3 and $Bi_2S_{2.75}Se_{0.25}$ are listed in Table 4. It can be seen from Table 4 that $\varepsilon_1(0)$ increased with the

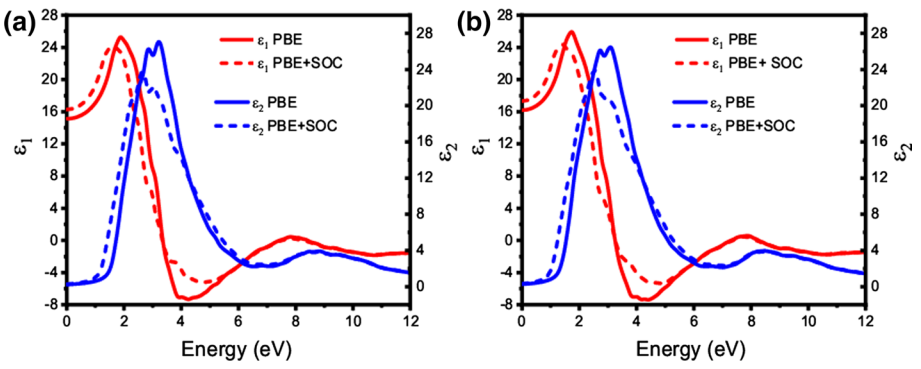

Fig. 6 Calculated real and imaginary parts of the dielectric function of Bi_2S_3 (**a**) and $Bi_2S_{2.75}Se_{0.25}$ with PBE and PBE + SOC method

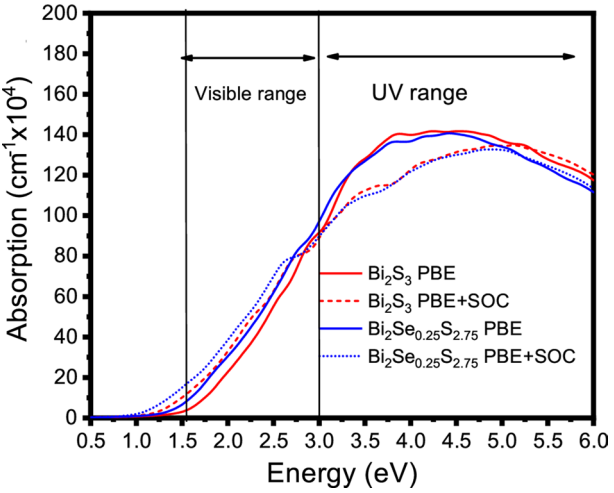

Fig. 7 Calculated absorption coefficient $\alpha(\omega)$ of Bi_2S_3 and $Bi_2S_{2.75}Se_{0.25}$ with PBE and PBE + SOC methods

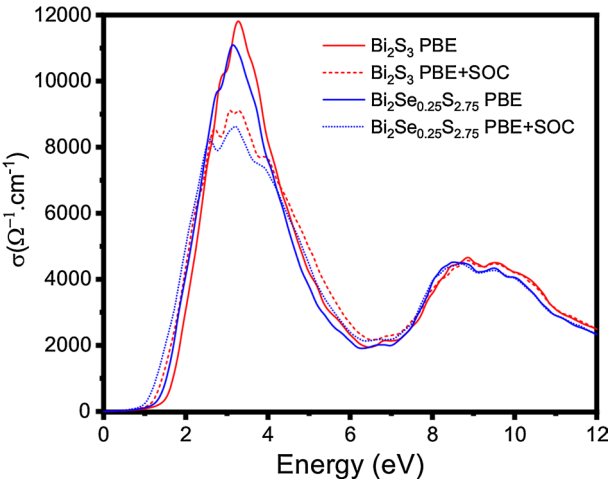

Fig. 8 Calculated optical conductivity $\sigma(\omega)$ of Bi_2S_3 and $Bi_2S_{2.75}Se_{0.25}$ with PBE and PBE + SOC methods

addition of the Se element and in the presence of the (SOC) giving rise to a high dielectric constant. To study the stability of the excitons, we calculate the exciton binding energy which can be calculated using the Bohr model (Bushick et al. 2019),

$$E_b = \frac{13.6\ \text{eV} \cdot \mu^*}{\varepsilon_\infty(0)^2} \tag{1}$$

where μ^* is the reduced mass given by: $\mu^* = \frac{m_e^* m_h^*}{(m_e^* + m_h^*)}$ and $\varepsilon_\infty(0)$ is the static dielectric constant computed without (SOC) and listed in Table 4. To evaluate μ^*, we considered the directionally averaged value for m_e^* and m_h^* given from the Table 3. Our calculated binding energy E_b for Bi_2S_3 and $Bi_2S_{2.75}Se_{0.25}$ are 74.16 meV and 29.10 meV respectively. The calculated values of E_b are of the same order as those of type II–VI compounds (Strzałkowski et al. 2013). The obtained results for E_b indicate that the incorporation of selenium (Se) atoms in the bismithinite Bi_2S_3 decreases the exciton binding energy which induces a

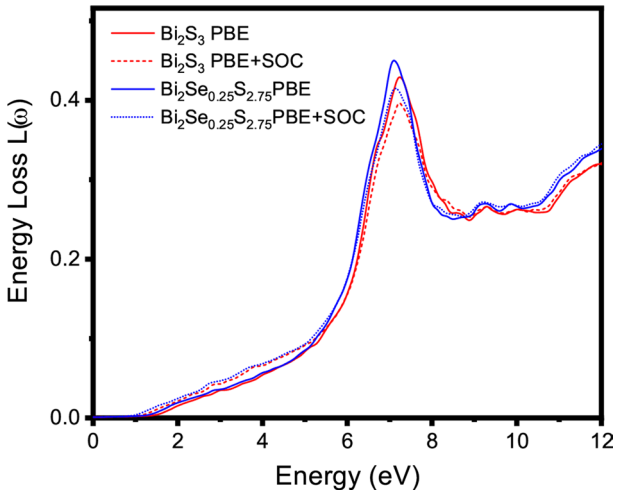

Fig. 9 Calculated energy loss function L(ω) of Bi_2S_3 and $Bi_2S_{2.75}Se_{0.25}$ with PBE and PBE + SOC methods

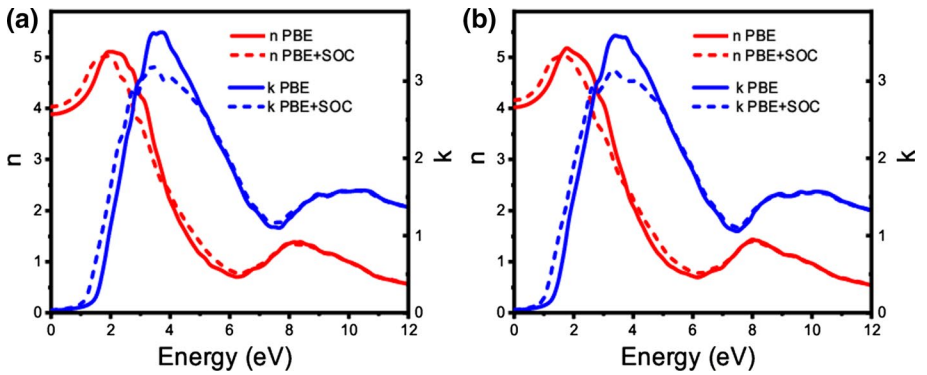

Fig. 10 Calculated complex refractive index $n(\omega)$ and extinction coefficient $k(\omega)$ of Bi_2S_3 (**a**) and $Bi_2S_{2.75}Se_{0.25}$ (**b**) with PBE and PBE + SOC methods

Table 4 Calculated optical constants for Bi_2S_3 and $Bi_2S_{2.75}Se_{0.25}$: static dielectric constant $\varepsilon_1(0)$, static refractive index $n(0)$, oscillator energy E_0, dispersion energy E_d and oscillator strength $\mathcal{F}$ calculated with and without SOC

Compound	Method	$\varepsilon_1(0)$	$n(0)$	E_0 (eV)	E_d (eV)	$\mathcal{F}$ (eV^2)
Bi_2S_3	Present (GGA-PBE)	14.981	3.886	2.866	40.429	115.869
	Present (PBE-SOC)	16.183	3.887	2.135	30.122	54.3100
$Bi_2S_{2.75}Se_{0.25}$	Present (GGA-PBE)	16.315	4.310	2.268	39.882	104.809
	Present (PBE-SOC)	17.375	4.157	2.214	36.061	79.8390

reduction in recombination, thus improving the efficiency of the extraction of the charge carriers.

It can be seen from Fig. 6a, b, that $\varepsilon_1(\omega)$ decrease to values below zero indicating that the reflection is maximum in the energy range about (3–7) eV and the materials exhibit

metallic behavior in this area. The absorptive part $\varepsilon_2(\omega)$ calculated with and without (SOC) for ($E\|z$) is illustrated in Fig. 6a, b for both compounds. $\varepsilon_2(\omega)$ spectra represent a pronounced peak located at 3.233 eV and 3.102 eV for Bi_2S_3 and $Bi_2S_{2.75}Se_{0.25}$ respectively, before the inclusion of the (SOC). With the inclusion of the (SOC), these high intensity peak of ε_2 show a red shift. A second peak, who is weaker than the first one, appears at 8.861 eV and 8.512 eV before and after inclusion of the (SOC) for Bi_2S_3 and $Bi_2S_{2.75}Se_{0.25}$ respectively. Thus, these differences in the results of the dielectric constants confirm the crucial role of SOC effects in the optical properties of undoped and doped Bi_2S_3. Our calculated maximum value of ε_2 for ($E\|z$) for Bi_2S_3 is in accordance with maximum peak values given theoretically by Sharma et al. (2012). It is known that $\varepsilon_2(\omega)$ is directly related to the optical electron transition. From PDOS displayed in Figs. 4 and 5 and for both compounds, the transition between the occupied states Bi 6s to unoccupied states S 3p is at the origin of the appearance of the main peaks, while the second peaks originates from transition occurring between Bi 6s and S 3p electrons. For $Bi_2S_{2.75}Se_{0.25}$ there is another transition between Se 3p and Bi 6p states participating in the appearance of the main peak in $\varepsilon_2(\omega)$.

The absorption coefficient $\alpha(\omega)$ spectra for ($E\|z$) calculated with and without (SOC) for Bi_2S_3 and $Bi_2S_{2.75}Se_{0.25}$ are given by Fig. 7. As can be seen from the $\alpha(\omega)$ spectra, the threshold of absorption is around 1.391 eV and 1.305 eV for undoped and doped Bi_2S_3 respectively. This shows that there was a shift towards low energies on the absorption edge with the incorporation of the Se atoms. This confirms the experimental results carried out on $Bi_2S_{3-x}Se_x$ (Chen et al. 2019). With the addition of (SOC), the threshold of absorption decrease and take the values of 1.192 eV and 1.010 eV for Bi_2S_3 and $Bi_2S_{2.75}Se_{0.25}$ respectively. The calculated energies of the threshold of absorption are close to the energy band gaps of Bi_2S_3 and $Bi_2S_{2.75}Se_{0.25}$ evaluated with and without the addition of (SOC) (see Table 2). In the energy range up to 3 eV, the absorption is maximum for $Bi_2S_{2.75}Se_{0.25}$ has a value of 94.79310^4 cm^{-1}, while at the same energy the undoped bismuthinite presents an absorption of the order of 90.22810^4 cm^{-1} in agreement with the experimental values ($104–10510^4$ cm^{-1}) (Rahman et al. 2016). This clearly shows that Bi_2S_3 becomes more absorbent in the visible range by doping it with selenium. For higher energy extending up to 3 eV, Bi_2S_3 crystal has a higher absorption than that of $Bi_2S_{2.75}Se_{0.25}$. The calculated high absorption coefficient of the ternary $Bi_2S_{2.75}Se_{0.25}$ shows that this material is very promising in photovoltaic applications. The addition of the (SOC) acts strongly on the absorption spectra particularly in the visible range where a slight shift is observed for both compounds. The optical conductivity σ(ω) describes the electron conduction produced by an incident photon crossing a material. The optical conductivity spectra for (E||z) calculated with and without addition of the (SOC) for both compounds are presented in Fig. 8. The optical conductivity presents a sharp peak in the visible range for both compounds Bi_2S_3 and $Bi_2S_{2.75}Se_{0.25}$. The maximum value of the optical conductivity decreases in the case of the calculation with (SOC) effect. L(ω) is the electron energy loss function describing the energy loss of a fast electron crossing a medium. The energy loss (Eloss) spectra for Bi_2S_3 and $Bi_2S_{2.75}Se_{0.25}$ calculated with and without (SOC) for (E||z) are given by Fig. 9. L(ω) present a prominent peak called the plasma resonance (Ouerghui et al. 2021a) located around 7.231 eV and 7.138 eV for Bi_2S_3 and $Bi_2S_{2.75}Se_{0.25}$ materials, respectively. The corresponding plasma frequencies are 10.98010^{15} Hz and 10.83910^{15} Hz. The calculated value of the plasma excitations for Bi_2S_3 is in accordance with theoretical results (Sharma et al. 2012) and experimental measurements (Nascimento et al. 1999).

The refractive index $n(\omega)$ and the extinction coefficient $k(\omega)$ for ($E\|z$) are plotted in the Fig. 10. It can be seen that $n(\omega)$ curves present an important value in low energy region

and remarkable reduction in high energy region. To analyze the refractive index at lower optical frequencies one can use the Wemple—DiDomenico (WDD) single-oscillator model (Ouerghui et al. 2021b) which is the most applied concept for the chalcogenide semiconductors. The (WDD) model is given by the following expression:

$$(n^2-1)^{-1} = \frac{E_0}{E_d} - \frac{1}{E_0 E_d}(h\nu)^2 \tag{2}$$

here, E_0 and E_d are the dispersion energy parameters, h is Planck's constant and hν is the photon energy.

The dispersion energy E_d corresponds to the dispersion of the electronic dielectric function related to the interband transition force, while E_0 is the single oscillator energy connected with the optical energy gap called WDD band gap (Ouerghui et al. 2021b). The dispersion parameters for Bi_2S_3 and $Bi_2S_{2.75}Se_{0.25}$ were estimated by fitting the plot $(n^2-1)^{-1}$ versus $(h\nu)^2$ in low energy region as shown in Fig. 11. Our calculated values of E_d and E_0 for Bi_2S_3 and $Bi_2S_{2.75}Se_{0.25}$ calculated with and without (SOC) are listed in Table 4. From Table 4, the dispersion energy E_d decreased while passing from Bi_2S_3 and $Bi_2S_{2.75}Se_{0.25}$ after and before the inclusion of (SOC). This is essential due to the addition of the Se atoms in Bi_2S_3 lattice which induced a weak force of the interband transitions. Similarly, the oscillatory energy E_0 decreases for $Bi_2S_{2.75}Se_{0.25}$ due to the decrease in the energy band gap. Based on the (WDD) model, we can calculate the static refractive index $n(0)$ from equation: $n(0) = \sqrt{1 + \left(\frac{E_d}{E_0}\right)}$. The static refractive indexes $n(0)$ for Bi_2S_3 and $Bi_2S_{2.75}Se_{0.25}$ calculated with and without (SOC) are given in Table 4. Another important parameter given by the WDD model is the oscillator strength given by: $\mathcal{F} = E_0 E_d$. The calculated values of $\mathcal{F}$ for Bi_2S_3 and $Bi_2S_{2.75}Se_{0.25}$ are reported in Table 4.

3.3.2 Non-linear optical parameters

The optical non-linearity of materials is directly related to the control of the light in optical switching devices. In the present work, the nonlinear optical properties (NLO) were studied from the calculation of the 3rd order nonlinear optical susceptibility $\chi^{(3)}$ and the

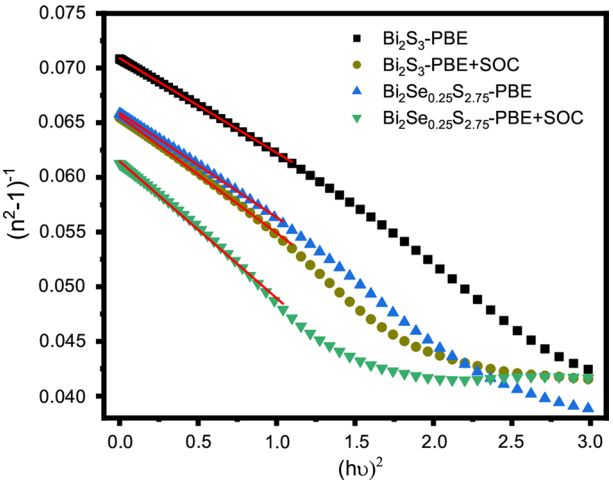

Fig. 11 $(n^2-1)^{-1}$ versus $(h\nu)^2$ $(h\nu)^2$ for Bi_2S_3 and $Bi_2S_{2.75}Se_{0.25}$ plotted with and without SOC

non-linear refractive index n_2 for Bi_2S_3 and $Bi_2S_{2.75}Se_{0.25}$ within the Miller's rule and the static refractive index $n(0)$ (Ouerghui et al. 2021b). It is known that the non-linearity occurs when the electromagnetic field becomes high enough. $\chi^{(3)}$ can be evaluated by the following expression:

$$\chi^{(3)} = \frac{A}{(4\pi)^4}\left(\frac{E_d}{E_0}\right)^4 \tag{3}$$

where A is a constant independent of the frequency and equal to 1.710^{-10} esu (Ouerghui et al. 2021b), E_d and E_0 are the dispersion parameters given by the (WDD) single-oscillator model. The non-linear refractive index n_2 is related to $\chi^{(3)}$ and the static refractive index n_0 which given by:

$$n_2 = \frac{12\pi\chi^{(3)}}{n(0)} \tag{4}$$

The calculated values of $\chi^{(3)}$ and n_2 for Bi_2S_3 and $Bi_2S_{2.75}Se_{0.25}$ are summarized in Table 5.

From Table 5, the calculated values of the (NLO) parameters $\chi^{(3)}$ and n_2 for Bi_2S_3 and $Bi_2S_{2.75}Se_{0.25}$ are large and this can be related to the electronic and geometrical structure of these two materials. The obtained value of $\chi^{(3)}$ coefficient of the bulk Bi_2S_3 is larger than measured experimentally for Bi_2S_3 nanocrystal: 6.2510^{-11} esu (Li et al. 2008). This difference is due in particular to the quantum confinement effect in the nanocrystals. In addition, the results presented in Table 5 show that doping Bi_2S_3 with Se atoms further expanded the (NLO) coefficients $\chi^{(3)}$ and n_2 thus showing the effect of Se doping Bi_2S_3 in improving the nonlinear optical properties and consequently in the realization of a promising nonlinear optical materials.

4 Conclusion

The effect of spin orbit coupling on the electronic and optical properties of $Bi_2S_{2.75}Se_{0.25}$ are investigated by means of Wien2k code based on the density functional theory. Firstly, the structural properties such as lattice constants, the bulk modulus and its pressure derivative of Bi_2S_3 and $Bi_2S_{2.75}Se_{0.25}$ are calculated within the PBE-GGA scheme. The calculated electronic band structures show that $Bi_2S_{2.75}Se_{0.25}$ is a direct band gap semiconductor with and without the inclusion of (SOC). The energy band gap reduction with respect to that of undoped Bi_2S_3 is due to the splitting states near the Fermi level if the (SOC) is taken into account. The carrier effective masses of Bi_2S_3 and $Bi_2S_{2.75}Se_{0.25}$ were calculated along high symmetry directions showing an increase in both the anisotropy and the

Table 5 Non-linear optical parameters: third-order nonlinear optical susceptibility $\chi^{(3)}$ and nonlinear refractive index n_2 for Bi_2S_3 and $Bi_2S_{2.75}Se_{0.25}$ calculated with and without (SOC)

Compound	Method	$\chi^{(3)}$ 10^{-10} (esu)	n_2 10^{-10} (esu)
Bi_2S_3	Present (GGA-PBE)	2.699	4.363
	Present (PBE-SOC)	2.701	4.369
$Bi_2S_{2.75}Se_{0.25}$	Present (GGA-PBE)	6.512	9.493
	Present (PBE-SOC)	4.797	7.493

carrier mobility when Se atoms were incorporated. The linear optical properties of Bi_2S_3 and Se doped Bi_2S_3 (dielectric function, absorption, optical conductivity and energy loss function) were investigated for polarization parallel to the z axis. All linear optical spectra show a red shift when incorporating Se atoms in Bi_2S_3 lattice and after inclusion of (SOC). $Bi_2S_{2.75}Se_{0.25}$ exhibits a high absorption coefficient in the visible region showing its potential use in future for applications in solar cells. The static dielectric constant increase in $Bi_2S_{2.75}Se_{0.25}$ with (SOC) effect giving rise to a decrease in the exciton binding energy. The oscillator parameters such as the oscillator energy, the dispersion energy and the static refractive index for both Bi_2S_3 and $Bi_2S_{2.75}Se_{0.25}$ materials were estimated using the (WDD) single-oscillator model. It was found that the inclusion of Se content in Bi_2S_3 leads to the increase of the static refractive index but a decrease in the oscillator parameters. The nonlinear optical properties (NLO) of doped and undoped Bi_2S_3 were also reported. A large values of (NLO) parameters were obtained for $Bi_2S_{2.75}Se_{0.25}$ indicating that it can be a useful device for all-optical communication and computer network. We strongly believe that our study on the electronic, linear and nonlinear optical properties of the ternary bismuth sulfide $Bi_2S_{2.75}Se_{0.25}$ is important for the development of a new high-performance optoelectronic materiel in the Bi-based compounds.

Authors contribution HBA Formal analysis, Methodology, Investigation, Writing-original draft, Supervision, Validation, Conceptualization WO Formal analysis, Validation, Investigation, Conceptualization, Writing—review & editing.

Declarations

Conflict of interest The authors declare that they have no known competing financial interests or personal relationships that could have appeared to influence the work reported in this paper.

References

Anasane, N., Ameta, R.: Morphologies of nanostructured bismuth sulphide and Mn(II) doped bismuth sulphide nanoparticles: characterization and application. Mater. Sci. Pol. **35**, 6–13 (2017). https://doi.org/10.1515/msp-2017-0032

Andzane, J., Kunakova, G., Varghese, J., Holmes, J.D., Erts, D.: Photoconductive properties of Bi2S3 nanowires. J. Appl. Phys. **117**, 064305 (2015). https://doi.org/10.1063/1.4907867

Bala, A., Nautiyal, T., Auluck, S.: Basic nanosystems of early 4d and 5d transition metals: electronic properties and the effect of spin-orbit interaction. J. Appl. Phys. **104**, 014302 (2008). https://doi.org/10.1063/1.2939251

Ben Abdallah, H., Bennaceur, R.: First-principles calculations of the electronic and optical properties of In6S7 compound. Physica b: Condens. Matter. **404**, 194–198 (2009). https://doi.org/10.1016/j.physb.2008.10.038

Ben Abdallah, H., Ouerghui, W.: Hybrid functional calculations of electro-optical properties of novel Ga1−xInxTe ternary chalcogenides. Appl. Phys. A Mater. Sci. Process. **126**, 1–12 (2020). https://doi.org/10.1007/s00339-020-03581-8

Bernechea, M., Cao, Y., Konstantatos, G.: Size and bandgap tunability in Bi2S3 colloidal nanocrystals and its effect in solution processed solar cells. J. Mater. Chem. A **3**, 20642–20648 (2015). https://doi.org/10.1039/c5ta04441c

Biswas, K., Zhao, L.D., Kanatzidis, M.G.: Tellurium-free thermoelectric: the anisotropic n -type semiconductor Bi 2S 3. Adv. Energy Mater. **2**, 634–638 (2012). https://doi.org/10.1002/aenm.201100775

Blaha, P., Schwarz, K., Tran, F., Laskowski, R., Madsen, G.K.H., Marks, L.D.: WIEN2k: an APW+lo program for calculating the properties of solids. J. Chem. Phys. **152**, 074101 (2020). https://doi.org/10.1063/1.5143061

Bushick, K., Mengle, K., Sanders, N., Kioupakis, E.: Band structure and carrier effective masses of boron arsenide: effects of quasiparticle and spin-orbit coupling corrections. Appl. Phys. Lett. **114**, 022101 (2019)

Caracas, R., Gonze, X.: First-principles study of the electronic properties of A2 B3 minerals, with A=Bi, Sb and B=S,Se. Phys. Chem. Miner. **32**, 295–300 (2005). https://doi.org/10.1007/s00269-005-0470-y

Chen, X., Hong, Y., Ge, X., Li, C., Miao, X., Wang, P., Zhang, Z., Yin, L.: Se-doped Bi2S3 nanoneedles grown on the three-dimensional carbon foam as a self-supported anode for high-performance sodium ion batteries. J. Alloys Compd. **825**, 153901 (2020). https://doi.org/10.1016/j.jallcom.2020.153901

Chen, Y., Wang, D., Zhou, Y., Pang, Q., Shao, J., Wang, G., Wang, J., Zhao, L.D.: Enhancing the thermoelectric performance of Bi2S3: a promising earth-abundant thermoelectric material. Front. Phys. **14**, 13601 (2019). https://doi.org/10.1007/s11467-018-0845-4

Cheng, H., Huang, B., Lu, J., Wang, Z., Xu, B., Qin, X., Zhang, X., Dai, Y.: Synergistic effect of crystal and electronic structures on the visible-light-driven photocatalytic performances of Bi2O3 polymorphs. Phys. Chem. Chem. Phys. **12**, 15468–15475 (2010). https://doi.org/10.1039/c0cp01189d

Chu, C.H., Leung, C.W.: The convolution equation of Choquet and Deny on [IN]-groups. Integral Equ. Oper. Theory **40**, 391–402 (2001). https://doi.org/10.1007/BF01198136

Deng, J., Zhao, Z.Y.: Electronic structure and optical properties of bismuth chalcogenides Bi2Q3 (Q = O, S, Se, Te) by first-principles calculations. Comput. Mater. Sci. **142**, 312–319 (2018). https://doi.org/10.1016/j.commatsci.2017.10.032

Du, X., Cai, F., Wang, X.: Enhanced thermoelectric performance of chloride doped bismuth sulfide prepared by mechanical alloying and spark plasma sintering. J. Alloys Compd. **587**, 6–9 (2014). https://doi.org/10.1016/j.jallcom.2013.10.185

Ellis, L.D., Wilkes, B.N., Hatchard, T.D., Obrovac, M.N..: In situ XRD study of silicon, lead and bismuth negative electrodes in nonaqueous sodium cells. J. Electrochem. Soc. **161**, A416–A421 (2014). https://doi.org/10.1149/2.080403jes

Ganose, A.M., Butler, K.T., Walsh, A., Scanlon, D.O.: Relativistic electronic structure and band alignment of BiSI and BiSeI: candidate photovoltaic materials. J. Mater. Chem. A **4**, 2060–2068 (2016). https://doi.org/10.1039/c5ta09612j

Ge, Z.H., Zhang, B.P., Liu, Y., Li, J.F.: Nanostructured Bi 2-xCu xS 3 bulk materials with enhanced thermoelectric performance. Phys. Chem. Chem. Phys. **14**, 4475–4481 (2012). https://doi.org/10.1039/c2cp23955h

Grigas, J., Talik, E., Lazauskas, V.: X-ray photoelectron spectra and electronic structure of Bi_2S_3 crystals. Phys. Stat. Sol. **230**, 220–230 (2002)

Guo, D., Hu, C., Zhang, C.: First-principles study on doping and temperature dependence of thermoelectric property of Bi2S3 thermoelectric material. Mater. Res. Bull. **48**, 1984–1988 (2013). https://doi.org/10.1016/j.materresbull.2013.02.004

Harman, T.C., Taylor, P.J., Walsh, M.P., LaForge, B.E.: Quantum dot superlattice thermoelectric materials and devices. Science **297**, 2229–2232 (2002). https://doi.org/10.1126/science.1072886

Hu, Y., Mao, L., Yuan, X., Lu, J., Chen, R., Chen, T., Zhang, W., Xue, X., Yan, W., Shokouhimehr, M., Zhang, X.L., Jin, Z.: Controllable growth and flexible optoelectronic devices of regularly-assembled Bi2S3 semiconductor nanowire bifurcated junctions and crosslinked networks. Nano Res. **13**, 2226–2232 (2020). https://doi.org/10.1007/s12274-020-2841-6

Kawamoto, Y., Iwasaki, H.: Thermoelectric properties of (Bi1-x Sb x) 2S3 with orthorhombic structure. J. Electron. Mater. **43**, 1475–1479 (2014). https://doi.org/10.1007/s11664-013-2742-5

Kim, J.H., Lim, T., Park, J.Y., Ma, A., Jung, H., Kim, H.Y., Cho, S.K., Yoon, H., Nam, K.M.: Understanding and improving photoelectrochemical performance of Bi2O3/Bi2S3 composite. New J. Chem. **43**, 11893–11902 (2019). https://doi.org/10.1039/c9nj02913c

Koc, H., Ozisik, H., Deligöz, E., Mamedov, A.M., Ozbay, E.: Mechanical, electronic, and optical properties of Bi2S 3and Bi2Se3 compounds: first principle investigations. J. Mol. Model. **20**, 2180 (2014). https://doi.org/10.1007/s00894-014-2180-1

Konstantatos, G., Levina, L., Tang, J., Sargent, E.H.: Sensitive solution-processed Bi2S3 nanocrystalline photodetectors. Nano Lett. **8**, 4002–4006 (2008). https://doi.org/10.1021/nl802600z

Li, C., Shi, G., Song, Y., Zhang, X., Guang, S., Xu, H.: Third-order nonlinear optical properties of Bi2S3 and Sb2S3 nanorods studied by the Z-scan technique. J. Phys. Chem. Solids. **69**, 1829–1834 (2008). https://doi.org/10.1016/j.jpcs.2008.01.012

Li, C., Zhao, J., Hu, Q., Liu, Z., Yu, Z., Yan, H.: Crystal structure and transporting properties of Bi2S3under high pressure: experimental and theoretical studies. J. Alloys Compd. **688**, 329–335 (2016). https://doi.org/10.1016/j.jallcom.2016.06.276

Liufu, S.C., Chen, L.D., Yao, Q., Wang, C.F.: Assembly of one-dimensional nanorods into Bi2S3 films with enhanced thermoelectric transport properties. Appl. Phys. Lett. **90**, 2012–2015 (2007). https://doi.org/10.1063/1.2712504

Miller, N.C., Bernechea, M.: Research update: bismuth based materials for photovoltaics. APL Mater. **6**, 084503 (2018). https://doi.org/10.1063/1.5026541

Mizoguchi, H., Hosono, H., Ueda, N., Kawazoe, H.: Preparation and electrical properties of Bi2S3 whiskers. J. Appl. Phys. **78**, 1376–1378 (1995). https://doi.org/10.1063/1.360315

Nascimento, V.B., De Carvalho, V.E., Paniago, R., Soares, E.A., Ladeira, L.O., Pfannes, H.D.: XPS and EELS study of the bismuth selenide. J. Electron Spectros. Relat. Phenomena. **104**, 99–107 (1999). https://doi.org/10.1016/s0368-2048(99)00012-2

Nordström, L., Madsen, G.K.H., Blaha, P., Schwarz, K., Sjöstedt, E.: Efficient linearization of the augmented plane-wave method. Phys. Rev. B **64**, 195134 (2001). https://doi.org/10.1103/PhysRevB.64.195134

Ouerghui, W., Alkhalifah, M.S.: Density functional investigation of structural, electronic, optical and thermodynamic properties of Zn1−xBexO semiconductor. Appl. Phys. A Mater. Sci. Process. **125**, 1–12 (2019). https://doi.org/10.1007/s00339-019-2664-z

Ouerghui, W., Alkhalifah, M.S., Abdallah, H.: Ben: DFT calculations on ZnO1−x compounds for optoelectronic applications. J. Comput. Electron. **20**, 467–479 (2021a). https://doi.org/10.1007/s10825-020-01645-9

Ouerghui, W., Gassoumi, M., Beji, L., Maaref, M.A.: Optical properties of quaternary GaMnAsP thin layer grown by molecular beam epitaxy. Physica E : Low-dimensional Systems and Nanostructures **131**, 114733 (2021). https://doi.org/10.1016/j.physe.2021.114733

Pejova, B., Grozdanov, I.: Structural and optical properties of chemically deposited thin films of quantum-sized bismuth(III) sulfide. Mater. Chem. Phys. **99**, 39–49 (2006). https://doi.org/10.1016/j.matchemphys.2005.10.010

Perdew, J.P., Burke, K., Ernzerhof, M.: Generalized gradient approximation made simple. Phys. Rev. Lett. **77**, 3865–3868 (1996). https://doi.org/10.1103/PhysRevLett.77.3865

Rabin, O., Perez, J.M., Grimm, J., Wojtkiewicz, G., Weissleder, R.: An X-ray computed tomography imaging agent based on long-circulating bismuth sulphide nanoparticles. Nat. Mater. **5**, 118–122 (2006). https://doi.org/10.1038/nmat1571

Rahman, A.A., Huang, R., Whittaker-Brooks, L.: Distinctive extrinsic atom effects on the structural, optical, and electronic properties of Bi2S3-xSex solid solutions. Chem. Mater. **28**, 6544–6552 (2016). https://doi.org/10.1021/acs.chemmater.6b02081

Sharma, Y., Srivastava, P., Dashora, A., Vadkhiya, L., Bhayani, M.K., Jain, R., Jani, A.R., Ahuja, B.L.: Electronic structure, optical properties and Compton profiles of Bi 2S 3 and Bi 2Se 3. Solid State Sci. **14**, 241–249 (2012). https://doi.org/10.1016/j.solidstatesciences.2011.11.025

Shubar, M.Y., Saadon, H.L., Abbas, S.J.: High-performance all-optical switching based on nonlinear response in semiconductor Bi2S3-xSex/PMMA nanocomposite films. Mater. Technol. **35**, 494–506 (2020). https://doi.org/10.1080/10667857.2019.1701253

Song, L., Chen, C., Zhang, S.: Preparation and photocatalytic activity of visible light-sensitive selenium-doped bismuth sulfide. Powder Technol. **207**, 170–174 (2011). https://doi.org/10.1016/j.powtec.2010.10.026

Song, H., Zhan, X., Li, D., Zhou, Y., Yang, B., Zeng, K., Zhong, J., Miao, X., Tang, J.: Rapid thermal evaporation of Bi2S3 layer for thin film photovoltaics. Sol. Energy Mater. Sol. Cells **146**, 1–7 (2016). https://doi.org/10.1016/j.solmat.2015.11.019

Strzałkowski, K., Zakrzewski, J., Maliński, M.: Determination of the exciton binding energy using photothermal and photoluminescence spectroscopy. Int. J. Thermophys. **34**, 691–700 (2013). https://doi.org/10.1007/s10765-012-1382-y

Whittaker-Brooks, L., Gao, J., Hailey, A.K., Thomas, C.R., Yao, N., Loo, Y.L.: Bi2S3 nanowire networks as electron acceptor layers in solution-processed hybrid solar cells. J. Mater. Chem. C **3**, 2686–2692 (2015). https://doi.org/10.1039/c4tc02534b

Wu, T., Zhou, X., Zhang, H., Zhong, X.: Bi2S3 nanostructures: a new photocatalyst. Nano Res. **3**, 379–386 (2010). https://doi.org/10.1007/s12274-010-1042-0

Yu, Y.Q., Zhang, B.P., Ge, Z.H., Shang, P.P., Chen, Y.X.: Thermoelectric properties of Ag-doped bismuth sulfide polycrystals prepared by mechanical alloying and spark plasma sintering. Mater. Chem. Phys. **131**, 216–222 (2011). https://doi.org/10.1016/j.matchemphys.2011.09.010

Zhang, B., Ye, X., Hou, W., Zhao, Y., Xie, Y.: Biomolecule-assisted synthesis and electrochemical hydrogen storage of Bi2S3 flowerlike patterns with well-aligned nanorods. J. Phys. Chem. B **110**, 8978–8985 (2006). https://doi.org/10.1021/jp060769j

Zhang, L.J., Zhang, B.P., Ge, Z.H., Han, C.G.: Fabrication and properties of Bi2S3-xSex thermoelectric polycrystals. Solid State Commun. **162**, 48–52 (2013). https://doi.org/10.1016/j.ssc.2013.03.013

Zhang, Y., Xu, J., Cui, Q., Yang, B.: Eu3+ -doped Bi4 Si3 O12 red phosphor for solid state lighting: microwave synthesis, characterization, photoluminescence properties and thermal quenching mechanisms. Sci. Rep. **7**, 42464 (2017). https://doi.org/10.1038/srep42464

Zhu, H., Pan, M., Johansson, M.B., Johansson, E.M.J.: High photon-to-current conversion in solar cells based on light-absorbing silver bismuth iodide. Chemsuschem **10**, 2592–2596 (2017). https://doi.org/10.1002/cssc.201700634